water

MDPI

Article

Physics-Informed Data-Driven Models to Predict Surface Runoff Water Quantity and Quality in Agricultural Fields

Jing Liang [1], Wenzhe Li [2], Scott A. Bradford [3] and Jiří Šimůnek [1,*]

[1] Department of Environmental Sciences, University of California, Riverside, CA 92521, USA; jing.liang@email.ucr.edu
[2] Department of Computer Sciences, University of Southern California, Los Angeles, CA 90089, USA; wenzheli@usc.edu
[3] USDA, ARS, US Salinity Laboratory, Riverside, CA 92507, USA; Scott.Bradford@ars.usda.gov
* Correspondence: jiri.simunek@ucr.edu; Tel.: +1-951-827-7854

Received: 28 December 2018; Accepted: 20 January 2019; Published: 24 January 2019

Abstract: Contaminants can be rapidly transported at the soil surface by runoff to surface water bodies. Physically-based models (PBMs), which are based on the mathematical description of main hydrological processes, are key tools for predicting surface water impairment. Along with PBMs, data-driven models are becoming increasingly popular for describing the behavior of hydrological and water resources systems since these models can be used to complement or even replace physically based-models. Here we propose a new data-driven model as an alternative to a physically-based overland flow and transport model. First, we have developed a physically-based numerical model to simulate overland flow and contaminant transport. A large number of numerical simulations was then carried out to develop a database containing information about the impact of various relevant factors on surface runoff quantity and quality, such as different weather patterns, surface topography, vegetation, soil conditions, contaminants, and best management practices. Finally, the resulting database was used to train data-driven models. Several Machine Learning techniques were explored to find input-output functional relations. The results indicate that the Neural Network model with two hidden layers performed the best among selected data-driven models, accurately predicting runoff water quantity and quality over a wide range of parameters.

Keywords: machine learning; surface runoff; contaminant transport; physically-based model; agriculture field; synthetic data; HYDRUS-1D

1. Introduction

A variety of agricultural pollutants resulting from farming and ranching operations (e.g., sediment, nutrients, pathogens, pesticides, metals, and salts) can lead to impairments of local and far-field water quality. These diffuse nonpoint sources can directly harm ecosystem and watershed water quality, and adversely affect our drinking water supply. Agricultural runoff, generated by rainfall or irrigation events, can transfer pollutants accumulated at the land surface into receiving water bodies. This process has been identified as one of the major causes of water impairment in agricultural settings [1–3]. The amount of pollutants transported to surface runoff water is dependent on local soil and crop management, climatic conditions, contaminant properties and environmental factors. The discharge of pollutants from agricultural activities to surface waters can be minimized by locally implementing Best Management Practices (BMPs). However, obtaining monitoring data using field investigations is very time consuming and expensive, and associated with many experimental difficulties. Furthermore, simple field observations may be difficult to interpret to obtain a complete picture of potential

contaminant transport routes and mechanisms, and to extrapolate findings to other environmental conditions and climates.

Alternatively, physically-based and data-driven models are potential tools for examining and optimizing the effects of land-use changes and BMPs on surface water quality [4–7]. Indeed, numerical experiments can be cheaply conducted using a physically-based model (PBM) to predict runoff water quality over a wide range of agricultural fields, weather patterns, and BMPs. PBMs explicitly account for main hydrologic and contaminant transport processes using mathematical descriptions. Complex numerical or analytical techniques are commonly used to solve these mathematical descriptions, which may require significant computational time as the spatial and temporal scale of the considered problem increases.

In contrast to PBMs, data-driven models are based on functional relationships between input and output variables. Artificial intelligence approaches, such as Machine Learning (ML) techniques, are increasingly being used in data-driven models to quantify input-output functional relations for complex systems in hydrology [7–19]. Several ML algorithms for modeling rainfall-runoff processes include Linear Regression (LR), K-Nearest Neighbor Regression (kNN), Feed-forward Neural Networks (NN), and Support Vector Machine (SVM) models [20–25]. The NN technique consists of a neural network with a single or multiple hidden layer (Deep Neural Network) to describe complex, nonlinear structures in data. NN with multiple hidden layers have been successfully applied in many commercial products that are already available to the public, such as computer vision and speech recognition, language translation, and self-driving cars [26–28]. While there are some studies investigating the applicability of NN with multiple hidden layers in hydrology/contaminant transport problems (e.g., [19,29–32]), only limited experience exists with using ML algorithms in environmental applications involving surface runoff water quantity and quality. It is thus important to investigate the strengths and limitations of data-driven models and compare their predictions with robust PBMs.

As discussed above, while PBMs are powerful tools for simulating spatial and temporal distributions of various physical and chemical environmental variables, they require large amounts of data and computational resources. On the other hand, machine learning algorithms trained using PBMs, or the so-called "metamodels" [33,34], make predictions almost instantly. The overall objective of this research thus was to investigate the limitations and strengths of ML-based metamodels in comparison with the HYDRUS overland flow module [35] in predicting contaminant loads in runoff water from agricultural fields. We synthetically generated an extensive database using the HYDRUS overland flow module that uses standard descriptions of overland flow and transport processes that have been extensively verified to properly represent real field processes (e.g., [35–39]). This numerically generated database was used to generate metamodels that contained information about the impact of a wide range of physical factors on surface runoff quantity and quality in agricultural fields. Inputs included information about the agricultural field (slope, length, and area), the soils (type, roughness, initial water content, and initial contaminant concentration), and precipitation events (rainfall intensity and duration). Outputs included the cumulative water volume and the contaminant mass in runoff water. This database was then used in conjunction with ML techniques to develop correlation relationships between model inputs and outputs using various ML algorithms.

2. Database Preparation

2.1. Physically-Based Model

The one-dimensional diffusion-wave and advection-dispersion equations, which are commonly used for describing overland flow and solute transport, respectively, have recently been implemented into the popular HYDRUS-1D code [35]. This code has previously been used to numerically solve the Richards equation, which simulates water flow, and the convection-dispersion equation, which simulates contaminant transport in the subsurface [40]. Recent studies indicated that the governing overland flow equation can be written in a similar mathematical formulation as the Richards

equation [35,41–43] so that existing numerical schemes of HYDRUS-1D can be used to solve the following 1D-diffusion wave equation:

$$\frac{\partial h}{\partial t} - \frac{\partial}{\partial x}\left(\frac{kh^{5/3}}{n_{man}\sqrt{S}}\frac{\partial(z_b + h)}{\partial x}\right) = R - I \tag{1}$$

where x is a space coordinate in direction of flow (L; where L denotes units of length), z_b is a vertical coordinate of the soil surface, t is time (T; where T denotes units of time), h is the surface water depth (L), R is rainfall or the irrigation rate (LT^{-1}), and I is the infiltration rate (LT^{-1}), S is the mean local slope (defined as dz_b/dx) (-), and k is a unit conversion factor ($L^{1/3}T^{-1}$). The parameter n_{man} is a Manning's roughness coefficient for overland flow, and it is dimensionless when k = 1 $m^{1/3}s^{-1}$ or has units of $TL^{-1/3}$ when k is not equal to unity. See the graphical abstract for a schematic of some of these variables.

In this work, the infiltration rate I is described using the Green-Ampt infiltration model [44]. This model is a simplified physically-based approach that is based on fundamental physics to describe the infiltration process as a function of the soil suction head, water content, and soil hydraulic conductivity:

$$I = K_S\left(\frac{\psi\Delta\theta}{F} + 1\right) \tag{2}$$

where ψ is the wetting front soil suction head (L), $\Delta\theta$ is the water content difference (L^3L^{-3}), K_S is the saturated hydraulic conductivity (LT^{-1}), and F is the cumulative depth of infiltration (L). The value of $\Delta\theta$ is defined by using the following equations:

$$\Delta\theta = \theta_e(1 - S_e) \tag{3}$$

$$S_e = \frac{\theta_i - (n - \theta_e)}{\theta_e} \tag{4}$$

$$\theta_e = n - \theta_r \tag{5}$$

where S_e is the effective saturation (-), θ_e is the effective water content (L^3L^{-3}), n is the porosity (L^3L^{-3}), θ_i is the initial water content (L^3L^{-3}), and θ_r is the residual water content (L^3L^{-3}).

Solute transport in overland flow is usually described using the advection-dispersion equation (ADE) of the form:

$$\frac{\partial hc}{\partial t} + \frac{\partial s}{\partial t} = \frac{\partial}{\partial x}\left(hD\frac{\partial c}{\partial x}\right) - \frac{\partial Qc}{\partial x} + h\phi + Rc_r - Ic \tag{6}$$

where c is the solute concentration in the aqueous phase (ML^{-3}; where M denotes units of mass), c_r is the concentration in rainfall water (ML^{-3}); s is the sorbed solute concentration at the soil surface area (ML^{-2}), D is the effective dispersion coefficient accounting for both molecular diffusion and hydrodynamic dispersion (L^2T^{-1}), ϕ is a sink/source term that accounts for various zero- and first-order or other reactions ($ML^{-3}T^{-1}$), and Q is the runoff flow rate (L^2T^{-1}). The parameter Q is given as:

$$Q = hU = -\frac{kh^{5/3}}{n_{man}\sqrt{S}}\frac{\partial(h + z)}{\partial x} \tag{7}$$

where U is a depth-averaged velocity (LT^{-1}) calculated using the Manning–Strickler uniform flow formula [41]. The effect of diffusion on the dispersion coefficient can often be ignored and in this case the value of D can be defined as the product of the dispersivity (λ, (L)) and U. Kinetic sorption/desorption between the solid and aqueous phases can be described using the following equation:

$$\frac{\partial s}{\partial t} = \omega(K_D c - s) \tag{8}$$

where K_D is the linear equilibrium partition coefficient (L) and ω is the first-order desorption rate coefficient (T^{-1}). The product of K_D and ω is proportional to the sorption rate coefficient. Details about the numerical solutions of flow and transport models are provided in the HYDRUS-1D manual [45].

2.2. Numerical Simulations

A large number of numerical simulations was carried out to develop a database containing information about the impact of various relevant factors on surface runoff quantity and quality. In agricultural settings, land surface contaminants can be easily picked up and transported by surface runoff or can seep into the soil by infiltration. Therefore, simulation scenarios considered in this work mainly focused on the transport of various contaminants in overland flow over different soil and land surfaces under different rainfall rates.

At first, numerous water flow simulations were run with various input parameters shown in Table 1. In order to build a realistic training database, a wide range of input parameter values was selected. In these simulations, precipitation was distributed uniformly over the land surface and lasted one hour. Historical records of precipitation frequency for the San Jacinto, CA watershed (http://hdsc.nws.noaa.gov/hdsc/pfds) were employed to generate precipitation-frequency estimates that were employed in simulations. Seven different percent probabilities of exceedance were selected: 1%, 2%, 4%, 10%, 20%, 50%, and 100%. Various agricultural field conditions were obtained by assigning different values of the Manning's roughness coefficient, slope, and length. As a result, 150 different field conditions (6 Manning's roughness coefficients × 5 slopes × 5 lengths) were considered. Additionally, four different initial water contents were considered: max(θ_r, 0.1), 0.2, 0.3, and the saturated water content (θ_s), for each soil type. Selected Green-Ampt infiltration parameters (soil porosity, residual water content, suction head, and hydraulic conductivity) were taken from Rawls et al. [46] (Table 2). In all water flow simulations, cumulative water volumes at the bottom outlet at 25 evenly spaced times were outputs. The resulting water flow database thus contained 2,310,000 entries (22 soils × 7 rainfall rates × 150 field conditions × 4 initial water contents × 25 print times).

Table 1. Input parameters used in the numerical simulations.

Input	Values
Rainfall intensity (cm day^{-1})	21.6, 28.8, 40.8, 52.8, 69.6, 86.4, 105.6
Manning's roughness coefficient	0.01, 0.02, 0.04, 0.07, 0.15, 0.24
Slope (-)	0.01, 0.02, 0.04, 0.08, 0.16
Length (m)	30, 60, 120, 240, 480
K_D (cm)	0.1, 0.5, 1, 1.5, 2
Initial water content, θ_i	max(θ_r, 0.1), 0.2, 0.3, θ_s

Table 2. Green-Ampt infiltration parameters for various standard and tilled* soil classes.

Texture	θ_s	θ_r	θ_e	ψ (cm)	K (cm s^{-1})
Sand	0.437	0.020	0.417	4.950	3.272×10^{-3}
Loamy Sand	0.437	0.036	0.401	6.130	8.306×10^{-4}
Sandy Loam	0.453	0.041	0.412	11.010	3.028×10^{-4}
Loam	0.463	0.029	0.434	8.890	9.444×10^{-5}
Silt Loam	0.501	0.015	0.486	16.680	1.806×10^{-4}
Sandy Clay Loam	0.398	0.068	0.330	21.850	4.167×10^{-5}
Clay Loam	0.464	0.155	0.309	20.880	2.778×10^{-5}
Silty Clay Loam	0.471	0.039	0.432	27.300	2.778×10^{-5}
Sandy Clay	0.430	0.109	0.321	23.900	1.667×10^{-5}
Silty Clay	0.470	0.047	0.423	29.220	1.389×10^{-5}
Clay	0.475	0.090	0.385	31.630	8.333×10^{-6}

* Tillage management: all five Green-Ampt infiltration parameters were increased by 20% over values of a corresponding textural class.

Solute transport simulations were subsequently conducted for the previously described water flow simulations. In these simulations, it was assumed that a unit concentration (c_i = 1 g/cm^2) of solute was initially distributed along the soil profile. Since the solute transport equation is a linear equation, the results obtained for a unit initial solute concentrations can be simply multiplied by other initial concentrations to get corresponding results. Runoff water generated by rainfall events "mobilized" solutes from the land surface and transported them to the bottom outlet of the field. The "mobilization" process was described using different sorption and desorption rates. The exchange of solute concentrations between solid and liquid phases is controlled by the overland water flow rate and kinetic sorption/desorption parameters (ω and K_D) in Equation (8). The kinetic sorption model approaches equilibrium conditions when ω is large, whereas non-equilibrium conditions prevail when ω is small and solute release is slow. In this study, the database considered transport processes and solute desorption for near-equilibrium conditions (ω = 8640 day^{-1}) to mitigate the complexity of these transport processes. Hence, two additional input parameters, variable K_D shown in Table 1 and constant ω = 8640 day^{-1}, were accounted for in these simulations. Solute transport simulations generated the output that included the cumulative solute mass at the bottom outlet at 25 evenly spaced times. The inclusion of two additional parameters to describe transport of mobilized solutes (K_D and ω) resulted in a database that was five times bigger than the water flow database. Furthermore, the variance in the solute transport database was higher than the water flow database.

3. Data-Driven Models

In this section, we briefly describe the data-driven models used in this paper. They are divided into two broad classes, linear and nonlinear models. The selected linear data-driven models include Linear Regression (LR) and Linear Support Vector Machine (SVM-L). Nonlinear models include K-Nearest Neighbor Regression (kNN), Support Vector Machines with nonlinear kernel (SVM-NL), and Deep Neural Networks (DNN) with different numbers of hidden layers. We used the previously generated synthetic databases from the PBM to train the selected data-driven models to predict surface runoff water quantity and quality. All these models were implemented using the open-source Scikit-learn and Keras Libraries in Python 3.5 (Python Software Foundation, Wilmington, DE, USA) [47,48].

3.1. Linear Regression

LR is the simplest ML model, which is often treated as the baseline method. It applies linear mapping to minimize the sum of least square errors between input data (either experimental or derived from a PBM model) and output data (of the regression model). Suppose we have a set of training data set (y_i, x_{ij}), where i =1, 2, 3, . . . , N and j =1, 2, 3, . . . , k. In here, i is the index for training samples in the data set, j is the index for the input parameters. A general linear regression problem can be developed by assuming that output variables y_i are influenced by input parameters x_{ij} as:

$$y_i = \beta_0 + \sum_{j=1}^{k} \beta_j x_{ij} + e_i \quad (9)$$

where β_j are regression coefficients, β_0 is intercept, and e_i represent a deviation between actual and predicted values. The ordinary least squares procedure seeks to minimize the total sum of the residuals. However, since this approach treats data as a matrix, the process will be very computational intensive when we have large data sets. Therefore, gradient-based optimization approaches, which optimize the values of the coefficients by iteratively minimizing the sum of the squared errors for each pair of input and output values are used here [49].

3.2. Support Vector Machine

The SVM is another widely used model for both classification and regression tasks. The SVM model was originally developed for classification problems to find a hyperplane, which can separate a

data set into one class from those of another class [50,51]. The SVM models have been successfully extended to solve regression problems by the introduction of the so-called ε-insensitive loss function. This loss function is used to penalize errors that are greater than the threshold ε (an insensitivity zone). A version of the SVM for regression problems is called support vector regression (SVR) and it depends on a subset of the training data. The ε-SVR aims to find the flattest regression function $f(x_{ij})$ that has at most a deviation ε from actual y_i for all training points x_{ij}:

$$f(x_{ij}) = \sum_{j=1}^{k} w_j x_{ij} + b_i \tag{10}$$

where w_j are weights and b_i is the bias term that should be estimated from the training data. One great benefit of using ε-SVR is the use of kernels, which inherently map the data into a nonlinear space depending on the chosen kernel function. Therefore, the above regression can be formulated as [52]:

$$f(x_{ij}) = \sum_{j=1}^{k} w_j \Phi(x_{ij}) + b_i \tag{11}$$

where $\Phi(x_{ij})$ denotes nonlinear transformation (kernel functions). Several nonlinear kernel functions are available, such as polynomial, radial basis, and sigmoid functions. In this study, we tested both SVR with linear (SVM-L) and nonlinear (SVM-NL) sigmoid kernel functions.

The optimization of ε-SVR is more complicated than the LR model because there is a linear constraint. In this case, the penalty factor C and the slack variables ξ_i and ξ_i^* are introduced to cope with infeasible constraints [51]. Hence, w_j and b_i are estimated by minimizing the following objective function:

$$\min \frac{1}{2}|w|^2 + C\sum_{i=1}^{n} (\xi_i + \xi_i{}^*) \tag{12}$$

subject to

$$\begin{cases} y_i - f(x_{ij}) - b_i \leq \varepsilon + \xi_i^* \\ f(x_{ij}) + b_i - y_i \leq \varepsilon + \xi_i \\ \xi_i,\ \xi_i{}^* \geq 0 \end{cases} \tag{13}$$

where $|w|^2 = \sum_{j=1}^{k} w_j^2$. The penalty factor C determines the trade-off between the flatness of the function $f(x_{ij})$ and the amount up to which deviations larger than ε are tolerated. The slack variables ξ_i and $\xi_i{}^*$ determine the degree to which data points will be penalized if the error is larger than ε.

3.3. K-Nearest Neighbor Regression

K-Nearest Neighbor (kNN) Regression is another machine learning method for regression problems. The kNN is a non-parametric regression type of analysis. Predictions are made by computing the distance between all the data points in the database and searching for the number of neighbors (K_{nn}) which are most similar to a new instance. Once the nearest-neighbor list is obtained, the prediction of output y is achieved by assigning weights to the contributions of the neighbors, so that the nearer neighbors contribute more to the average than the more distant ones. For example, the Euclidean distance d between lth training sample x_{lj} and ith test sample x_{ij} is defined as [53]:

$$d(x_{ij}, x_{lj}) = \sqrt{\sum_{j=1}^{k} (x_{ij} - x_{lj})^2} \tag{14}$$

The weight w_d can be defined by a selected K_{nn} value and a distance between lth and ith samples:

$$w_d(x_{ij}, x_{lj}) = \frac{\exp(-d(x_{ij}, x_{lj}))}{\sum_{l=1}^{K_{nn}} \exp(-d(x_{ij}, x_{lj}))} \quad (15)$$

Thus, the output y_i can be predicted by

$$y_i = \sum_{l=1}^{K_{nn}} w_d(x_{ij}, x_{lj}) y_l \quad (16)$$

3.4. Deep Feed-Forward Network

Neural networks (NN) are the most popular ML models used nowadays. The classical feed-forward network is a neural network that has been widely used in the hydrologic and water quality problems [22,23,54–56]. The fundamental components of these algorithms include the input layer, intermediate layers, output layer, and neurons. Adjustable parameters characterize the neurons that are connected to the input and transmit the information from one neuron to another in one direction: from an input layer, through one or more hidden layers, to an output layer. Figure 1 illustrates the adjustable parameters for an individual neuron. In a network, the input variables x_{ij} are weighted and summed up to produce the hidden neurons S_p ($p = 1, 2, \ldots, P$):

$$S_p = \sum_{j=1}^{k} w_{jp} x_{ij} \quad (17)$$

where p is the number of hidden neurons. A neuron computes an output, based on the weighted sum of all its inputs (S_p), according to an activation function ($f(S_p)$). Finally, an activation function, which is applied to S_p, provides the final output from this logistic sigmoid [10] (see Figure 1). The sigmoid activation function is given as:

$$f(S_p) = \frac{1}{1 + e^{-S_p}} \quad (18)$$

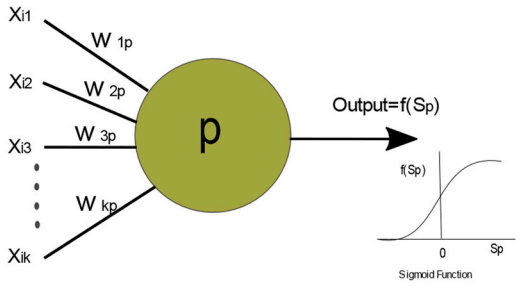

Figure 1. Activation of a single neuron.

The so-called Deep Neural Networks (DNN) model is a direct extension of the feed-forward network that contains multiple hidden layers that are stacked as shown in Figure 2 [57]. The DNN model becomes "deeper" as the number of hidden layers increases. Deeper NN models allow for simulating more complicated, nonlinear mapping functions between input and output data. However, DNN models often suffer from overfitting when using too many hidden layers. This problem can be mitigated by dropping layers. We have tested the DNN model with one, two, and three hidden layers to determine the optimum number of hidden layers and to minimize overfitting.

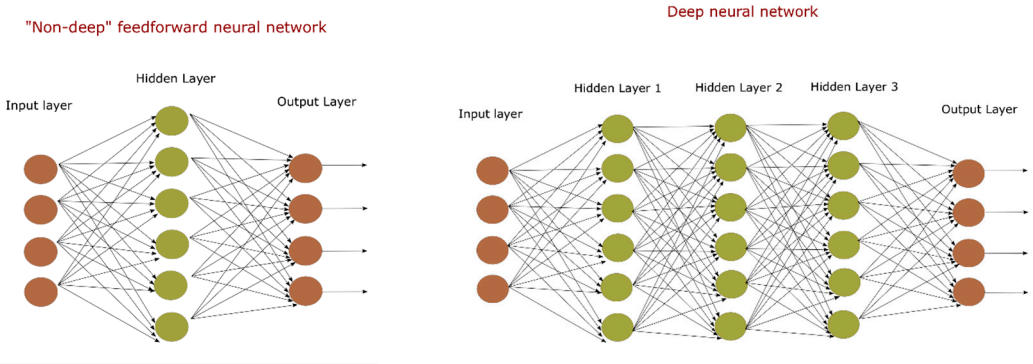

Figure 2. A feed-forward neural network (a single hidden layer, **left**) and a deep feed-forward neural network (multiple hidden layers, **right**).

4. Model Training and Evaluation

The runoff water database generated using the PBM was divided into training (80% of the entire database) and test (20% of the entire database) data sets for the data-driven models. Variable input parameters and output values were used to train the data-driven models by randomly selecting 18 out of 22 soil types. Each data-driven model was tuned using cross validation and further evaluated using the left-out test data set. After the training was completed, data-driven models were tested on the remaining four soil types over many different scenarios. The accuracy and predictive capability were first assessed by making scatter plots of cumulative runoff water volumes (Q_c) for data-driven models and the PBM. The calculated R^2 and the best-fitted regression line were shown in these scatter plots to quantify the goodness of the data-driven model prediction.

In addition, two examples were chosen to show the accuracy between observed and predicted cumulative runoff hydrographs between the PBM and data-driven models, respectively, over a range of initial water contents and soil types. The first example considered four different initial water contents and the following conditions: the rainfall rate of 69.6 cm/day for 1 h, the surface length of 240 m, a Silt Loam soil, the Manning's roughness coefficient of 0.24 (dense grass), and a steep slope of 16%. The total simulation time was 1 h and 10 min so that the water recession process could be fully captured in these simulations. The second example considered surface runoff from Silt Loam, Clay, tilled Silt Clay, and tilled Clay soils under the following conditions: an initially saturated soil, the rainfall rate of 105.4 cm/day for 1 h, a surface length of 48 m, a slope of 16%, and the Manning's roughness coefficient of 0.24.

Statistical measures were used to quantify the ability of various ML models to predict an output from the PBMs. Calculated statistical parameters included the root mean square error (RMSE), the mean absolute error (MAE), the mean bias error (MBE), the model efficiency (EF), and the *Relative Error* Δ_i. These statistical parameters were determined as:

$$\text{RMSE} = \sqrt{\frac{\sum_{i=1}^{N} (O_i - P_i)^2}{N}} \tag{19}$$

$$\text{MAE} = \frac{\sum_{i=1}^{N} |O_i - P_i|}{N} \tag{20}$$

$$\text{MBE} = \frac{\sum_{i=1}^{N} (O_i - P_i)}{N} \tag{21}$$

$$\text{EF} = 1 - \frac{\sum_{i=1}^{N} (O_i - P_i)^2}{\sum_{i=1}^{N} (O_i - \overline{O_i})^2} \tag{22}$$

$$Relative\ Error\ \Delta_i = \frac{(P_i - O_i)}{\frac{(P_i + O_i)}{2}} \quad (23)$$

where P_i and O_i are the output values predicted by data-driven models and observed data obtained from the PBM, respectively, $\overline{O}_i$ is the average of observed data, and N is the number of observations. It should be noted that data with zero values of surface runoff were removed from this analysis for model inter-comparison.

A database for transport of mobilized solute with runoff water (e.g., the cumulative solute mass at the outlet) was developed using the PBM that encompassed a wide range in rainfall rates, soil physical properties, initial water contents, slopes, field size, Manning's roughness coefficients, and kinetic sorption/desorption parameters. As we mentioned before, the solute transport database in this study considered transport processes and solute desorption for near-equilibrium conditions with a constant desorption rate coefficient (ω = 8640 day^{-1}) and different K_D values. The solute transport database had a similar structure as the water flow database but was five times bigger in size.

The contaminant transport is highly related to water flow. The data-driven model with the best performance in predicting the runoff water volume was therefore selected for training with the solute transport databases. Data-driven models were trained against 80% of the entire solute transport database using Q_c, K_D, and other input parameters associated with the water flow database. The remaining 20% of the solute transport database were employed for testing the model. Two simulation examples were chosen to further investigate the predictive ability of the trained data-driven models. These simulation scenarios considered the same input variables as for the water flow model (e.g., differences in initial water contents or soil texture) with K_D = 2 cm and ω = 8640 day^{-1}.

5. Results and Discussion

5.1. Surface Runoff Quantity

5.1.1. Linear Regression

A scatter plot of estimated Q_c using the LR model versus observed Q_c for the PBM test data set are shown in Figure 3a. We can see that R^2 is equal to 0.439, which indicates that the LR model failed to accurately describe the PBM data. The LR algorithm usually works well with high-bias and low variance data. However, the PBM describes real-world scenarios with complex, nonlinear relationships between input and output variables that generate high variance data sets.

The observed (PBM) runoff water volume in Figure 3b decreased and was increasingly delayed when the initial soil water content was lower. The observed (PBM) simulations in Figure 3c demonstrate that the Clay and tilled Clay textured soils produced the most runoff water because of their lower saturated hydraulic conductivity and infiltration. After rainfall stops, the cumulative runoff water flux continues to increase because water flows slowly over the rough surface before reaching the bottom boundary. The LR model failed to accurately describe runoff water dynamic for these two selected examples, especially when the initial water content was higher (Figure 3b) and the hydraulic conductivity was lower (Figure 3c). In particular, the LR model tended to overestimate Q_c for early times and underestimate Q_c for later times. Other authors (e.g., [18]) similarly found that the linear regression model does not provide enough flexibility to represent complex nonlinear hydrological phenomena.

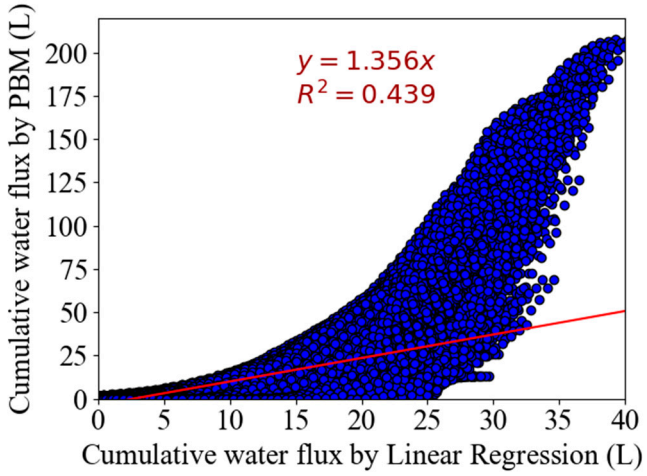

(**a**)

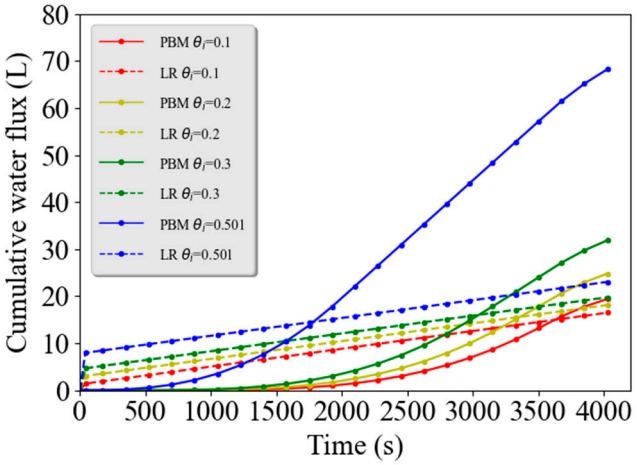

(**b**)

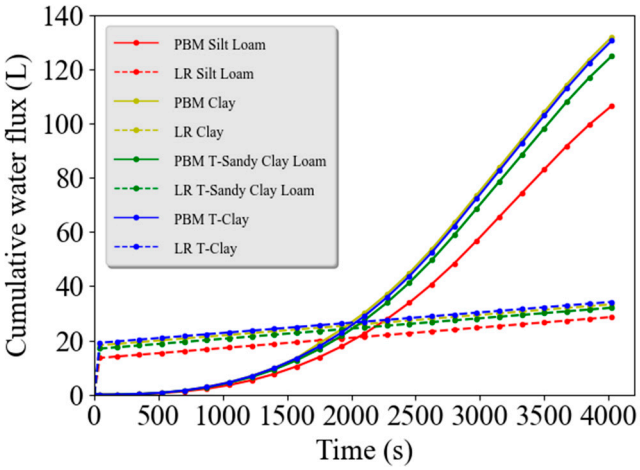

(**c**)

Figure 3. Comparison of cumulative water fluxes (Q_c in liters, L) calculated by the physically-based models PBM and the Linear Regression (LR) model ((**a**) overall, (**b**) different initial water contents, (**c**) different textures)).

5.1.2. Support Vector Machine

Similar to the LR model, the Support Vector Machine model with linear kernel functions (SVM-L) produced a linear input-output relationship. Two user-defined parameters for the SVM-L model were the penalty parameter C on the error term, which was set to 1, and the maximum number of iterations, which was 2000 [58]. Figure 4a indicates that this SVM-L model had an even lower R^2 (R^2 = 0.386) than the LR model (R^2 = 0.439). Similarly, simulation examples shown in Figure 4b (different initial water contents) and 4c (different textures) indicate that the SVM-L model completely failed to capture the large values of Q_c at later times. Linear models (LR and SVM-L) are therefore not well suited to describe complex nonlinear runoff problems.

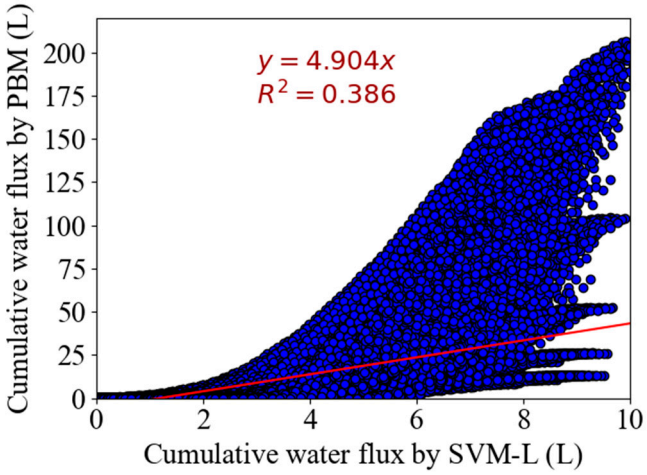

(**a**)

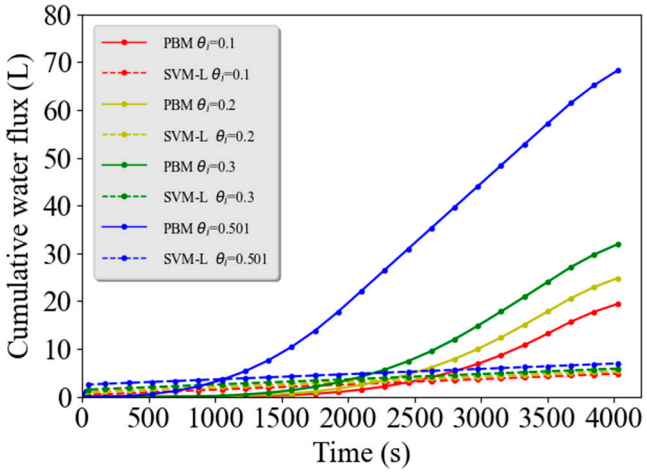

(**b**)

Figure 4. *Cont.*

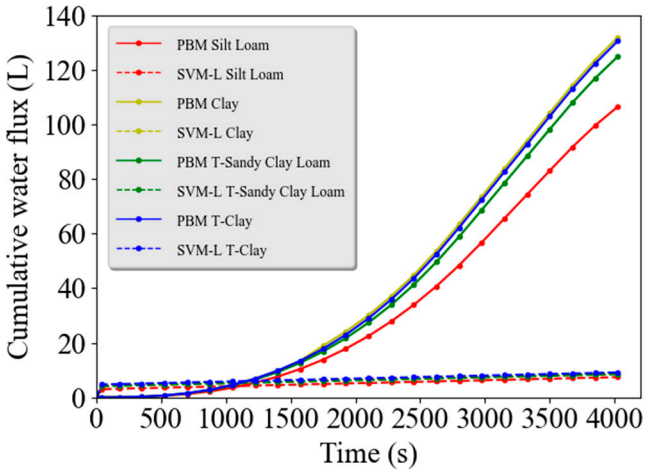

(**c**)

Figure 4. Comparison of cumulative water fluxes (Q_c in liters, L) calculated by the PBM and the Linear Support Vector Machine (SVM-L) model ((**a**) overall, (**b**) different initial water contents, (**c**) different textures)).

Many researchers have indicated that the SVM model with nonlinear kernels (SVM-NL) can successfully describe surface/subsurface hydrology problems [18,59,60]. However, previous SVM-NL applications have considered only a relatively small training and test data set. Training the SVM-NL model takes a tremendous amount of computational time because of the complexity of this model. For example, we estimated that training the SVM-NL model to our complete runoff water database would take somewhere between a few days and a month. Consequently, only about 20% of the original runoff water training data set were randomly selected to train the SVM-NL model. The trained model was then used for testing against the test data set with $C = 1$ and $\varepsilon = 0.2$. Figure 5a shows the scatter plot of estimated Q_c using the SVM-NL model versus observed Q_c from the test set. The R^2 ($R^2 = 0.952$) for the SVM-NL model was much higher than for the LR and SVM-L models. The SVM-NL model also provided a much-improved description of the PBM results for the two examples shown in Figure 5b,c. However, there were still considerable deviations between the SVM-NL model and the PBM, especially for larger print times, higher initial water contents (Figure 5b), and for the Silt Loam soil (Figure 5c).

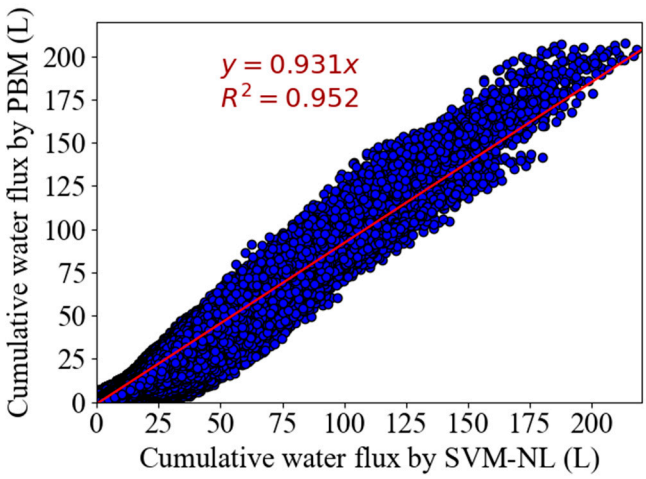

(**a**)

Figure 5. *Cont.*

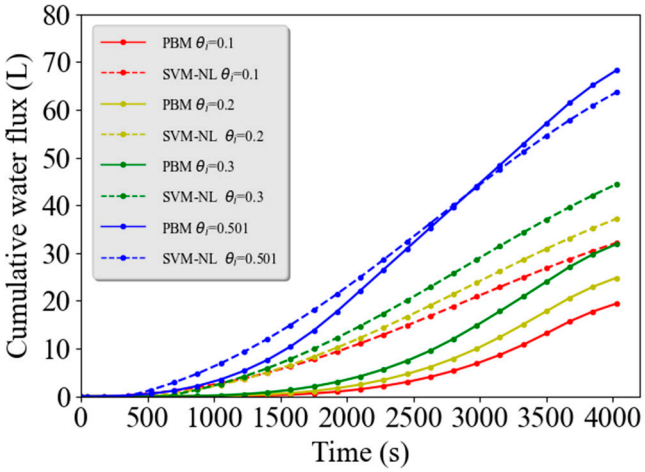

(**b**)

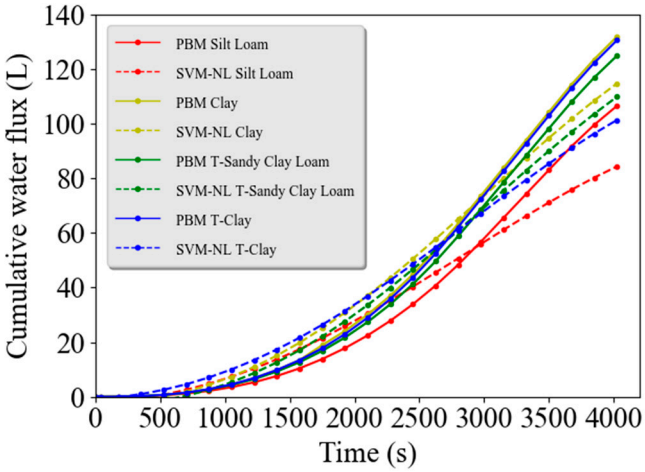

(**c**)

Figure 5. Comparison of cumulative water fluxes (Q_c in liters, L) calculated by the PBM and the Nonlinear Support Vector Machine (SVM-NL) model ((**a**) overall, (**b**) different initial water contents, (**c**) different textures)).

5.1.3. K-Nearest Neighbor Regression

The kNN models with different numbers of neighbors (the *K* value) were tested while all points in each neighborhood were weighted equally. We observed that the optimal *K* value is equal to 5. The results of calculations with the kNN model are summarized in Figure 6. The R^2 (R^2 = 0.957) for the kNN-5 model was slightly higher than that for the SVM-NL model (R^2 = 0.952). However, there were more predicted outliers when the observed Q_c was relatively small. Although the overall runoff trends were correctly captured in Figure 6b, the kNN-5 model underestimated the cumulative water flux at every print time and incorrectly predicted that Q_c stopped increasing when rainfall ended. Furthermore, this deviation tended to increase for smaller initial water contents. However, Figure 6c shows that the kNN-5 model did a much better job of predicting large values of Q_c than the SVM-NL model.

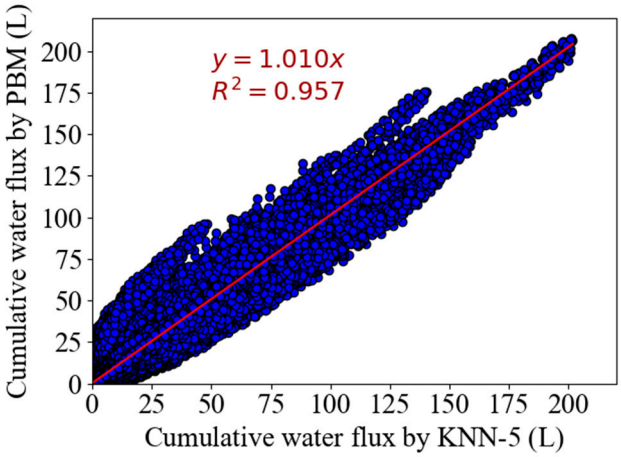

(**a**)

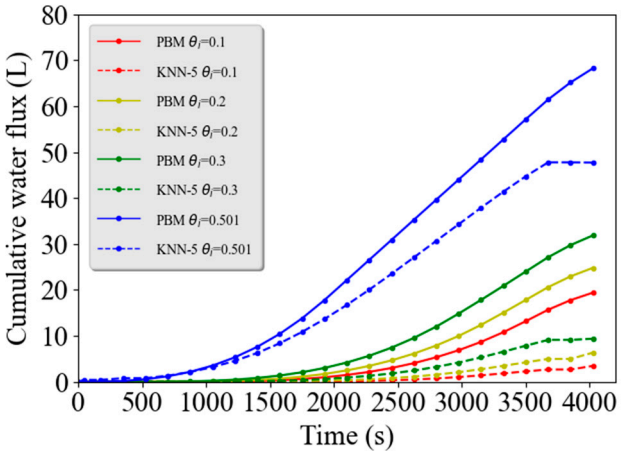

(**b**)

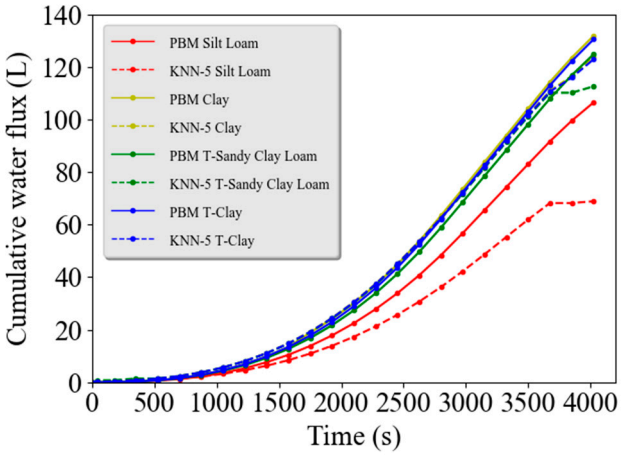

(**c**)

Figure 6. Comparison of cumulative water fluxes (Q_c in liters, L) calculated by the PBM and the k-Nearest Neighbor Regression (kNN-5) model ((**a**) overall, (**b**) different initial water contents, (**c**) different textures)).

5.1.4. Deep Feed-Forward Neural Network

The DNN models with one, two, and three hidden layers were tested to determine the optimum number of hidden layers and to minimize overfitting. In this study, the optimal number of neurons in each hidden layer was determined by trial and error. We tested possible numbers of neuron from 3 to 20 to see if the model performance was improved. The R^2 and the Root Mean Squared Error (RMSE) were not improved when neuron numbers were increased beyond 16. Therefore, the number of neurons in each hidden layer was set to 16.

Figure 7a shows the scatter plot of estimated Q_c using DNN models with three different layers versus observed Q_c for the PBM data set. Values of R^2 were equal to 0.978, 0.981, and 0.959 for the DNN-1, DNN-2, and DNN-3 models, respectively. The DNN models provided a description of runoff that was fairly accurate and obtained higher R^2 values than the other ML models. However, the top and bottom rows of Figure 7 indicate that the DNN-1 and DNN-3 models tended to underestimate and overestimate observed values of Q_c, respectively, whereas the DNN-2 model provided the best prediction. This result suggests that the one hidden layer model was not "deep" enough, whereas a three-layer model probably was too complicated and results in overfitting. A more quantitative comparison of various ML models is given below.

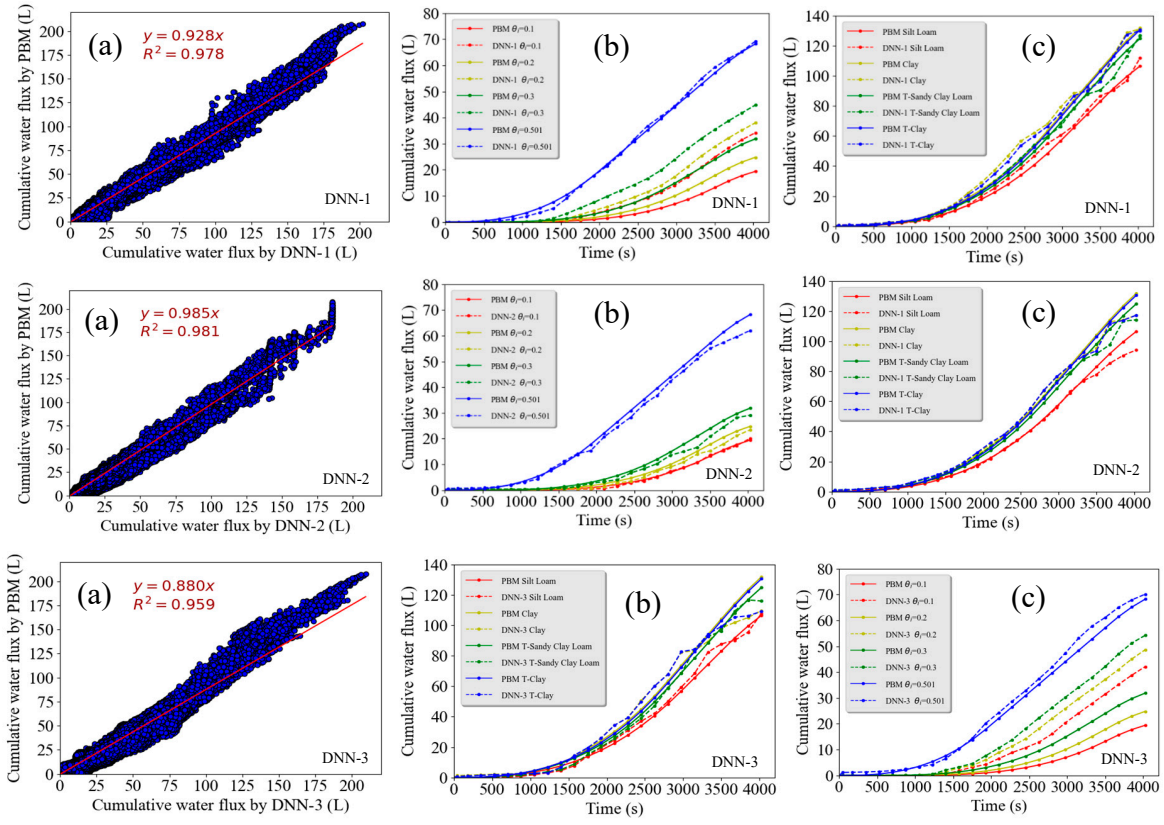

Figure 7. Comparison of cumulative water fluxes (Q_c in liters, L) calculated by the PBM and the Deep Feed-Forward Neural Network (DNN-1 (**top row**), DNN-2 (**middle row**), and DNN-3 (**bottom row**)) models ((**a**) overall, (**b**) different initial water contents, (**c**) different textures)).

5.1.5. Comparison of Data-Driven Models

Figure 8 presents a box plot of the relative error distribution for various data-driven models, as well as other statistical parameters for their agreement with the PBM. The LR and SVM-L models show big error distributions, which indicates that these models were not well suited to predict runoff. The SVM-NL model performed much better than the SVM-L and LR models, but not as well as kNN-5 and DNN models. It is possible that the performance of the SVM-NL model could be further improved

if the training data size was increased, but this would also dramatically increase the computational time. The boxplot of relative errors for the kNN-5 model was narrow, but it included a lot of outliers which indicated that the model performance may be different under other conditions. Figures 7a and 8 indicate that outliers of the relative error for DNN-1 appeared when Q_c was over 100 L, whereas the DNN-3 model slightly underestimated large Q_c values. The DNN-2 model shows the narrowest box plot of relative errors and the best performance statistics for the considered ML models. This indicates that the DNN-2 model provided the best prediction of runoff water volumes.

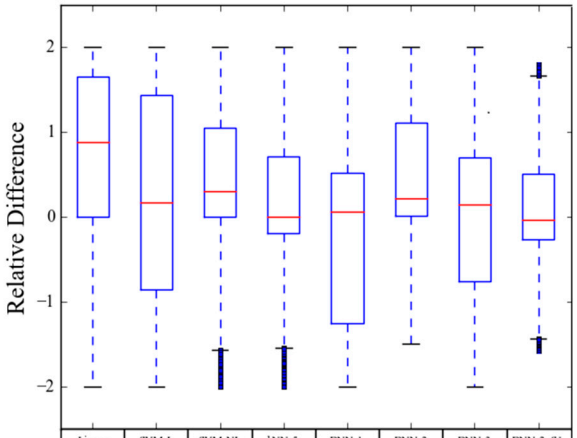

	Linear	SVM-L	SVM-NL	kNN-5	DNN-1	DNN-2	DNN-3	DNN-2_S1
RMSE	1.46	1.84	0.47	0.59	0.49	0.30	0.91	4.77
MAE	0.83	0.75	0.25	0.23	0.27	0.14	0.42	1.57
MBE	0.18	-0.57	0.21	0.13	0.19	0.10	0.35	0.18
EF	0.39	0.03	0.94	0.90	0.93	0.97	0.76	0.96

Figure 8. Statistical parameters associated with the trained data-driven models of runoff quantity and quality. The root mean square error (RMSE), mean bias error (MBE), mean absolute error (MAE), model efficiency (EF), and a box plot of the relative error distribution for data-driven models are given. The units of RMSE, MBE, and MAE of the runoff quantity and quality are liters and g, respectively. The upper and lower boundaries of the boxes show the 75th and 25th percentile, the whiskers of the box plot show the maximum and minimum values, and the red line within the box is the median value. Blue dot symbols indicated the outliers.

5.2. Surface Runoff Quality

We discovered that the DNN-2 model structure with fine adjusted model parameters performs best among all selected data-driven models for predicting the runoff water volume. We therefore trained the DNN-2 model with the near equilibrium solute transport database. The DNN-2 model for water flow could be directly adjusted to produce a data-driven model that relates physical factors and the cumulative solute mass.

Figure 9a presents a scatter plot of the cumulative solute mass predicted by the DNN-2 model and observed by the PBM under near equilibrium conditions. The constructed DNN-2 relationship between input and output variables for near equilibrium conditions was very accurate. The goodness of the DNN-2 predictions for solute transport near equilibrium conditions is reflected by the statistical parameters (RMSE = 4.77 g, MAE =1.57 g, MBE = 0.18 g, and EF = 0.96 g) in Figure 8, the value R^2 = 0.992 in Figure 9a, and the agreement between observed (PBM) and predicted results for the example simulations for various water contents (Figure 9b) and soil types (Figure 9c).

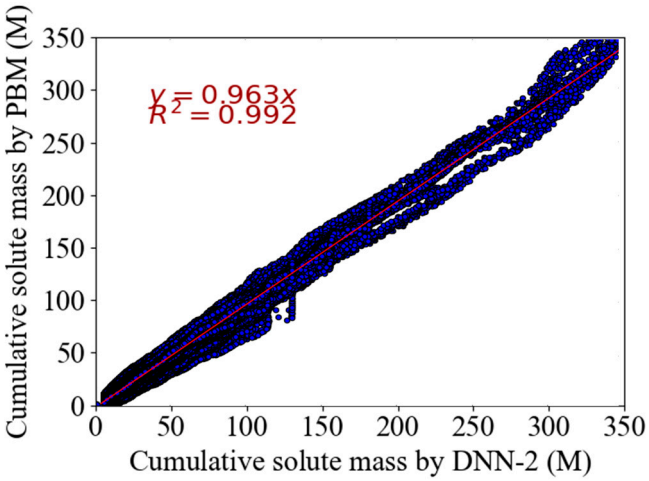

(**a**)

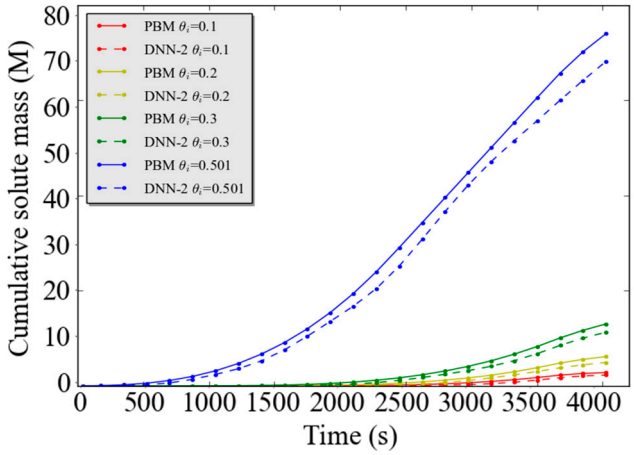

(**b**)

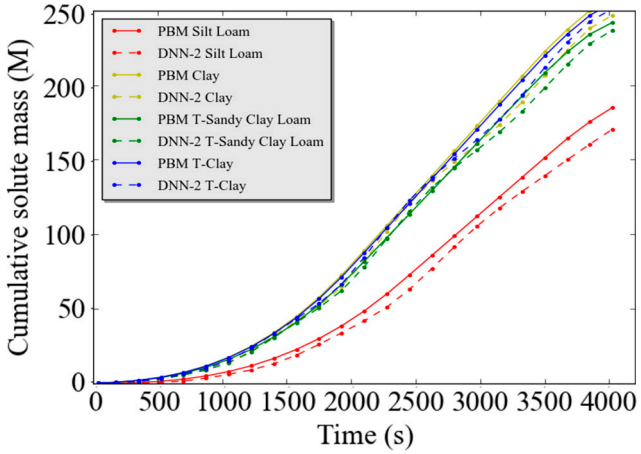

(**c**)

Figure 9. Comparison of the cumulative solute mass (in grams, M) calculated by the PBM and the DNN-2 model for the near equilibrium training data set ((**a**) overall, (**b**) different initial water contents, (**c**) different textures)).

6. Conclusions and Outlook

This study tested the ability of data-driven models to mimic PBMs to predict surface runoff water quantity and quality in agricultural settings. A physically-based overland flow and transport model was used to develop a large database containing information about the impact of various factors on surface runoff quantity and quality. In order to build a realistic training database, a wide range of input parameter values was selected. The input factors included: (a) rainfall intensities (for seven different percent probabilities of exceedance of 1%, 2%, 4%, 10%, 20%, 50%, and 100% for the San Jacinto Watershed, Southern California), (b) Manning's roughness coefficients (reflecting management practices; 6 values), (c) field slopes (5 values), (d) field lengths (5 values), (e) soil properties (affecting infiltration; 11 soil types with and without tillage), (f) initial water contents (4 values), and (g) solute sorption parameters (5 conditions). The resulting water flow database thus contained 2,310,000 entries, whereas the solute transport database was 5 times larger.

Multiple data-driven models were tested on their ability to relate/correlate model inputs with outputs. The following data-driven models were used in the analysis: Linear Regression (LR), k-Nearest Neighbor Regression (kNN), Support Vector Machine with linear (SVM-L) and nonlinear (SVM-NL) kernels, and Deep Neural Networks (DNN) (Neural Networks with multiple hidden layers). The LR and SWM-L models failed to accurately describe runoff water dynamics, having the regression coefficient (R^2) less than 0.5. In particular, both linear models tended to overestimate the runoff water volume for early times and underestimate it for later times. Both SVM-NL and kNN models performed much better than linear models, having R^2 of 0.93 and 0.96, respectively. However, there were still considerable deviations between the SVM-NL and kNN models and PBM predictions, especially for larger times, higher initial water contents, and for some textures (such as Silt Loam). Finally, the DNN models with one, two, and three hidden layers (DNN-1, DNN-2, and DNN-3) were tested to determine the optimum number of hidden layers and to minimize overfitting of output variables. The best performance was obtained by the DNN model with two hidden layers (DNN-2) (R^2 = 0.98). The DNN-1 and DNN-3 models tended to underestimate, and overestimate observed values of runoff water volumes, respectively.

In conclusion, DNN techniques exhibited a better capability to reproduce the results of the PBM compare with traditional ML techniques. In particular, results indicate that the simple linear models are not well suited to develop correlations for runoff from agricultural lands because runoff is a complex nonlinear hydrological process. Although nonlinear models like kNN and SVM-NL can fairly accurately capture the surface water flow dynamic, the DNN models are more promising for dealing with complex hydrologic problems. Applications of the DNN models with additional hidden layers provide a possibility to further improve the model performance. Similarly, the trained DNN-2 model provided an excellent prediction of near equilibrium solute transport.

It should be noted that the training databases from the PBM could also be augmented to include real monitoring data and/or more complex model formulations (e.g., multidimensional simulations, stochastic simulations, other reactive transport processes, and physical non-equilibrium flow and transport). This approach would preserve the benefits of data-driven models over PBMs (e.g., faster execution times and ability to incorporate real data), while constraining data-driven models to the underlying physics of hydrological processes.

Author Contributions: J.L. contributed to the development of the physically based and machine learning models, the data analysis, and the manuscript writing. W.L. contributed to the machine learning models and the data analysis. S.A.B. and J.Š. contributed to the physically based model, the data analysis, and the manuscript writing.

Funding: This research was supported by the USDA, ARS, National Program 211 and the Western Riverside County Agricultural Coalition (WRCAC). Although partial funding for this work was provided by WRCAC, no site-specific data from the San Jacinto Watershed have been used in this publication.

Conflicts of Interest: The authors declare no conflict of interest.

References

1. Carpenter, S.R.; Caraco, N.F.; Correll, D.L.; Howarth, R.W.; Sharpley, A.N.; Smith, V.H. Nonpoint pollution of surface waters with phosphorus and nitrogen. *Ecol. Appl.* **1998**, *8*, 559–568. [CrossRef]
2. United States Geological Survey (USGS). *The Quality of Our Nation's Waters-Nutrients and Pesticides*; US Geological Survey Circular 1225: Washington, DC, USA, 1999; p. 80.
3. Tyrrel, S.F.; Quinton, J.N. Overland flow transport of pathogens from agricultural land receiving faecal wastes. *J. Appl. Microbiol.* **2003**, *94*, 87–93. [CrossRef]
4. Kirkby, M.J.; Beven, K.J. A physically based, variable contributing area model of basin hydrology. *Hydrol. Sci. J.* **1979**, *24*, 43–69.
5. Donigian, A.S.; Love, J.T. The Connecticut Watershed Model—A tool for BMP impact assessment. *Proc. Water Environ. Fed.* **2002**, *2*, 605–624. [CrossRef]
6. Borah, D.K.; Bera, M. Watershed-scale hydrologic and nonpoint-source pollution models: Review of mathematical bases. *Trans. ASAE* **2003**, *46*, 1553. [CrossRef]
7. Roz, E.P. *Water Quality Modeling and Rainfall Estimation: A Data Driven Approach*; The University of Iowa: Iowa City, IA, USA, 2011.
8. Hsu, K.L.; Gupta, H.V.; Sorooshian, S. Artificial neural network modelling of the rainfall-runoff process. *Water Resour. Res.* **1995**, *31*, 2517–2530. [CrossRef]
9. Minns, A.W.; Hall, M.J. Artificial neural network as rainfall-runoff model. *Hydrol. Sci. J.* **1996**, *41*, 399–417. [CrossRef]
10. Dawson, C.W.; Wilby, R. An artificial neural network approach to rainfall-runoff modelling. *Hydrol. Sci. J.* **1998**, *43*, 47–66. [CrossRef]
11. Dibike, Y.B.; Solomatine, D.; Abbott, M.B. On the encapsulation of numerical-hydraulic models in artificial neural network. *J. Hydraul. Res.* **1999**, *37*, 147–161. [CrossRef]
12. Abrahart, R.J.; See, L. Comparing neural network and autoregressive moving average techniques for the provision of continuous river flow forecast in two contrasting catchments. *Hydrol. Process.* **2000**, *14*, 2157–2172. [CrossRef]
13. Mjolsness, E.; DeCoste, D. Machine learning for science: State of the art and future prospects. *Science* **2001**, *293*, 2051–2055. [CrossRef] [PubMed]
14. Govindaraju, R.S.; Rao, A.R. *Artificial Neural Networks in Hydrology*; Springer Science & Business Media: Berlin, Germany, 2013.
15. Solomatine, D.P.; Ostfeld, A. Data-driven modelling: Some past experiences and new approaches. *J. Hydroinform.* **2008**, *10*, 3–22. [CrossRef]
16. Remesan, R.; Mathew, J. *Hydrological Data Driven Modelling: A Case Study Approach*; Springer: Berlin, Germany, 2014; Volume 1.
17. Bai, Y.; Chen, Z.; Xie, J.; Li, C. Daily reservoir inflow forecasting using multiscale deep feature learning with hybrid models. *J. Hydrol.* **2016**, *532*, 193–206. [CrossRef]
18. Karandish, F.; Šimůnek, J. A comparison of numerical and machine-learning modeling of soil water content with limited input data. *J. Hydrol.* **2016**, *543*, 892–909. [CrossRef]
19. Fang, K.; Shen, C.; Kifer, D.; Yang, X. Prolongation of SMAP to Spatiotemporally Seamless Coverage of Continental US Using a Deep Learning Neural Network. *Geophys. Res. Lett.* **2017**, *44*, 11-030. [CrossRef]
20. Loague, K.M.; Freeze, R.A. A comparison of rainfall-runoff modeling techniques on small upland catchments. *Water Resour. Res.* **1985**, *21*, 229–248. [CrossRef]
21. Karlsson, M.; Yakowitz, S. Nearest-neighbor methods for nonparametric rainfall-runoff forecasting. *Water Resour. Res.* **1987**, *23*, 1300–1308. [CrossRef]
22. ASCE Task Committee on Application of Artificial Neural Networks in Hydrology. Artificial neural networks in hydrology—I: Preliminary concepts. *J. Hydrol. Eng.* **2000**, *5*, 115–123. [CrossRef]
23. ASCE Task Committee on Application of Artificial Neural Networks in Hydrology. Artificial neural networks in hydrology—II: Hydrologic applications. *J. Hydrol. Eng.* **2000**, *5*, 124–137. [CrossRef]
24. Lin, J.Y.; Cheng, C.T.; Chau, K.W. Using support vector machines for long-term discharge prediction. *Hydrol. Sci. J.* **2006**, *51*, 599–612. [CrossRef]
25. Nourani, V.; Komasi, M.; Mano, A. A multivariate ANN-wavelet approach for rainfall–runoff modeling. *Water Resour. Manag.* **2009**, *23*, 2877–2894. [CrossRef]

26. Hinton, G.; Deng, L.; Yu, D.; Dahl, G.E.; Mohamed, A.R.; Jaitly, N.; Senior, A.; Vanhoucke, V.; Nguyen, P.; Sainath, T.N.; et al. Deep neural networks for acoustic modeling in speech recognition: The shared views of four research groups. *IEEE Signal Process. Mag.* **2012**, *29*, 82–97. [CrossRef]
27. LeCun, Y.; Bengio, Y.; Hinton, G. Deep learning. *Nature* **2015**, *521*, 436. [CrossRef] [PubMed]
28. Goodfellow, I.; Bengio, Y.; Courville, A.; Bengio, Y. *Deep Learning*; MIT Press: Cambridge, UK, 2016; Volume 1.
29. Sahoo, G.B.; Ray, C.; Mehnert, E.; Keefer, D.A. Application of artificial neural networks to assess pesticide contamination in shallow groundwater. *Sci. Total Environ.* **2006**, *367*, 234–251. [CrossRef]
30. Stenemo, F.; Lindahl, A.M.L.; Gärdenäs, A.; Jarvis, N. Meta-modeling of the pesticide fate model MACRO for groundwater exposure assessments using artificial neural networks. *J. Contam. Hydrol.* **2007**, *93*, 270–283. [CrossRef] [PubMed]
31. Fienen, M.N.; Nolan, B.T.; Feinstein, D.T. Evaluating the sources of water to wells: Three techniques for metamodeling of a groundwater flow model. *Environ. Model. Softw.* **2016**, *77*, 95–107. [CrossRef]
32. Marçais, J.; de Dreuzy, J.R. Prospective interest of deep learning for hydrological inference. *Groundwater* **2017**, *55*, 688–692. [CrossRef] [PubMed]
33. Blanning, R.W. The construction and implementation of metamodels. *Simulation* **1975**, *24*, 177–184. [CrossRef]
34. Schoumans, O.F.; Mol-Dijkstra, J.; Akkermans, L.M.W.; Roest, C.W.J. SIMPLE: Assessment of non-point phosphorus pollution from agricultural land to surface waters by means of a new methodology. *Water Sci. Tech.* **2002**, *45*, 177–182. [CrossRef]
35. Liang, J.; Bradford, S.A.; Šimůnek, J.; Hartmann, A. Adapting HYDRUS-1D to simulate overland flow and reactive transport during sheet flow deviations. *Vadose Zone J.* **2017**, *16*, 18. [CrossRef]
36. Ahuja, L.R.; Sharpley, A.N.; Lehman, O.R. Effect of Soil Slope and Rainfall Characteristics on Phosphorus in Runoff. *J. Environ. Qual.* **1982**, *11*, 9–13. [CrossRef]
37. Sharda, V.N.; Singh, S.R.; Sastry, G.; Dhruvanarayana, V.V. A finite element model for simulating runoff and soil erosion from mechanically treated agricultural lands: 2. Field validation and applications. *Water Resour. Res.* **1994**, *30*, 2299–2310. [CrossRef]
38. Wallach, R.; Grigorin, G.; Rivlin, J. A comprehensive mathematical model for transport of soil-dissolved chemicals by overland flow. *J. Hydrol.* **2001**, *247*, 85–99. [CrossRef]
39. Goodrich, D.C.; Burns, I.S.; Unkrich, C.L.; Semmens, D.J.; Guertin, D.P.; Hernandez, M.; Yatheendradas, S.; Kennedy, J.R.; Levick, L.R. KINEROS2/AGWA: Model use, calibration, and validation. *Trans. ASABE* **2012**, *55*, 1561–1574. [CrossRef]
40. Šimůnek, J.; Van Genuchten, M.T.; Šejna, M. Recent developments and applications of the HYDRUS computer software packages. *Vadose Zone J.* **2016**, *15*, 25. [CrossRef]
41. Hromadka, T.V., II; Lai, C. Solving the two-dimensional diffusion flow model. In *Hydraulics and Hydrology in the Small Computer Age, Proceedings of the Specialty Conference on Hydraulics and Hydrology in the Small Computer Age, Lake Buena Vista, FL, USA, 12–17 August 1985*; ASCE: New York, NY, USA, 1985; pp. 555–562.
42. Panday, S.; Huyakorn, P.S. A fully coupled physically-based spatially-distributed model for evaluating surface/subsurface flow. *Adv. Water Resour. Res.* **2004**, *27*, 361–382. [CrossRef]
43. Weill, S.; Mouche, E.; Patin, J. A generalized Richards equation for surface/subsurface flow modelling. *J. Hydrol.* **2009**, *366*, 9–20. [CrossRef]
44. Green, W.H.; Ampt, G.A. Studies in soil physics. I. The flow of air and water through soils. *J. Agric. Sci.* **1911**, *4*, 1–24.
45. Šimůnek, J.; Šejna, M.; Saito, H.; Sakai, M.; van Genuchten, M.T. *The HYDRUS-1D Software Package for Simulating the Movement of Water, Heat, and Multiple Solutes in Variably Saturated Media*, Version 4.0. HYDRUS Software Series 3, Department of Environmental Sciences, University of California Riverside: Riverside, CA, USA, 2008; 315.
46. Rawls, W.J.; Brakensiek, D.L.; Miller, N. Green-Ampt infiltration parameters from soils data. *J. Hydrol. Eng.* **1983**, *109*, 62–70. [CrossRef]
47. Pedregosa, F.; Varoquaux, G.; Gramfort, A.; Michel, V.; Thirion, B.; Grisel, O.; Blondel, M.; Prettenhofer, P.; Weiss, R.; Dubourg, V.; et al. Scikit-learn: Machine learning in Python. *J. Mach. Learn. Res.* **2011**, *12*, 2825–2830.
48. Chollet, F. Keras: Deep Learning Library for Theano and Tensorflow. 2015. Available online: https://keras.io/ (accessed on the 21 January 2019).

49. Ticlavilca, A.M.; McKee, M. Multivariate Bayesian regression approach to forecast releases from a system of multiple reservoirs. *Water Resour. Manag.* **2011**, *25*, 523–543. [CrossRef]
50. Vapnik, V.N. *Statistical Learning Theory*; Wiley: New York, NY, USA, 1998.
51. Vapnik, V. *The Nature of Statistical Learning Theory*; Springer Science & Business Media: Berlin, Germany, 2013.
52. Van Looy, K.; Bouma, J.; Herbst, M.; Koestel, J.; Minasny, B.; Mishra, U.; Montzka, C.; Nemes, A.; Pachepsky, Y.; Padarian, J.; et al. Pedotransfer functions in Earth system science: Challenges and perspectives. *Rev. Geophys.* **2017**, *55*, 1199–1256. [CrossRef]
53. Friedman, J.; Hastie, T.; Tibshirani, R. *The Elements of Statistical Learning*; Springer Series in Statistics: Berlin, Germany, 2001; Volume 1, pp. 337–387.
54. Maier, H.; Dandy, G.C. Neural networks for the prediction and forecasting of water resources variables: A review of modeling issues and applications. *J. Environ. Model. Softw.* **2000**, *15*, 101–124. [CrossRef]
55. Sharma, V.; Negi, S.C.; Rudra, R.P.; Yang, S. Neural networks for predicting nitrate-nitrogen in drainage water. *Agric. Water Manag.* **2003**, *63*, 169–183. [CrossRef]
56. Khalil, B.; Ouarda, T.B.M.J.; St-Hilaire, A. Estimation of water quality characteristics at ungauged sites using artificial neural networks and canonical correlation analysis. *J. Hydrol.* **2011**, *405*, 277–287. [CrossRef]
57. Schmidhuber, J. Deep learning in neural networks: An overview. *Neural Netw.* **2015**, *61*, 85–117. [CrossRef] [PubMed]
58. Joachims, T. *Learning to Classify Text Using Support Vector Machines: Methods, Theory and Algorithms*; Kluwer Academic Publishers: Norwell, MA, USA, 2002; Volume 186.
59. Dibike, Y.B.; Velickov, S.; Solomatine, D.; Abbott, M.B. Model induction with support vector machines: Introduction and applications. *J. Comput. Civ. Eng.* **2001**, *15*, 208–216. [CrossRef]
60. Bray, M.; Han, D. Identification of support vector machines for runoff modelling. *J. Hydroinform.* **2004**, *6*, 265–280. [CrossRef]